INTERNATIONAL JOURNAL of RENEWABLE ENERGY RESEARCH
D. M. Bui et al., Vol.16, No.2, June, 2026

A Novel Statistical and Adaptive Current and Voltage-Based Fault Protection Scheme Developed for Off-grid Low-Voltage DC Microgrids

Duong Minh Bui*‡, Danh Hoang Le**, Hieu Minh Nguyen***, Phuc Duy Le****

*Faculty of Engineering, Vietnamese-German University, Ho Chi Minh City, Vietnam
**Faculty of Electrical and Electronics Technology, Ho Chi Minh City University of Industry and Trade, Ho Chi Minh City, Vietnam
***Faculty of Engineering, Vietnamese-German University, Ho Chi Minh City, Vietnam
****Faculty of Electrical Engineering, Industrial University of HCM City, Ho Chi Minh City, Vietnam

(duong.bm@vgu.edu.vn, hoangdanh0407@gmail.com, hieu.nm@vgu.edu.vn, phucld91@gmail.com)

‡Corresponding Author: Duong Minh Bui, Vietnamese-German University, Ho Chi Minh City, Vietnam, Tel: +84-918 163356, duong.bm@vgu.edu.vn

Received: 18. 02. 2024 Accepted: 08. 04. 2024

Abstract- This paper presents a novel fault protection scheme for standalone low-voltage (LV) DC microgrids (MG), which relies on the first-order current and voltage derivatives to detect pole-to-pole (P2P) and pole-to-ground (P2G) faults in the system. Local measurements of current and voltage signals are applied for the proposed protection scheme. To effectively adapt to high noise levels of current and voltage sensors from the local measurements, a Chi-square-based statistic method is developed to determine tripping thresholds of the current and voltage derivatives in this proposed protection scheme. To be highly adaptable to the directional change of fault currents in the DC microgrid, moreover, the standard deviation- and mean-based calculation of lower and upper boundaries of current and voltage parameters has been also applied for the protection system. As a new contribution of the paper, this novel statistical and adaptive current- and voltage-based protection system can be more effective in protecting source and load branches of the small-scaled LVDC microgrid. Specifically, irrespective of large transients and measurement noises during the standalone operation of DC MGs, different P2P and P2G faults can be detected and cleared within a few milliseconds. The protection design procedure for DC microgrids is also detailed in this paper. For high applicability, solid-state relays and microcontrollers are equipped for the off-grid $48V_{DC}$ microgrid testbed to implement and validate the suggested novel fault protection algorithm by doing multiple staged-fault tests at different positions in this microgrid testbed.

Keywords Chi-square threshold, current derivative, DC microgrid, voltage derivative, fault current, islanded operation.

1. Introduction

A direct-current microgrid mainly consists of DC-power-consumed loads, DC-power-generating sources like photovoltaic (PV) arrays, and energy storage systems (ESS) [1, 2]. The DC microgrid technology uses fewer power-conversion stages as compared to the AC microgrid [3]. Moreover, the operation of multiple parallel converter-based distributed generators (DG) can be an easier task in the DC microgrid as compared to the AC microgrid due to ignoring synchronization conditions and reactive power control requirements [4]. However, the operation of a DC microgrid can face fault-related challenges because power converters and loads in the DC microgrid can be susceptible to extremely high fault currents from DC-link capacitors in the system [5, 6]. Therefore, a fast and adaptive protection system is needed to limit the negative impact of fault disturbances on the operation of DC microgrids by detecting and clearing different faults within the expected time frame.

Faults in an LVDC microgrid can be classified into short-circuit faults or arc faults [7]. A short-circuit event can either happen between lines (or poles), creating a line-to-line (or called pole-to-pole (P2P)) fault, or between the line and the ground, creating a line-to-ground (or called pole-to-ground (P2G)) fault. The lines in the DC microgrid are categorized further into positive or negative lines. In addition, arc faults normally occur in high-voltage DC microgrids due to deterioration of components, random weather conditions, and

lack of maintenance. For P2P faults, the microgrid's components can be susceptible to extremely high fault currents from DC-link capacitors of DC/DC or AC/DC power converters. Depending on different microgrid configurations and grounding systems, a P2G fault can be either a low-impedance or high-impedance fault, which adds another layer of the protection challenge to be overcome in developing an accurate and adaptive protection scheme for LVDC microgrids.

In [8-10], the authors discuss overcurrent-based protection schemes by comparing the measured current value with its tripping threshold to detect the P2P fault in the DC microgrid, with a relatively fast operation time. However, the overcurrent (OC) relay may be not properly activated under current transients because of the fast discharging of DC-link capacitors in the DC system [11]. In [12], it presents a local measurement method using the rate of current change to detect the fault in a ring-topology LVDC microgrid. However, threshold settings of the first-order and second-order current derivatives are only based on the pre-fault voltage, time interval, line loading, and equivalent impedance from the source to the faulted location, without considering the historical dynamic data of the change rates of current and voltage in the off-grid LVDC microgrid. Furthermore, the noise level of sensors can also complicate the accurate calculation of current/voltage derivatives, which may cause the maloperation of the protection. In [13, 14], overcurrent- and undervoltage-based protection solutions are proposed for the DC microgrid. In [15], a communication-supported overcurrent protection system for PV-based DC microgrids is developed by using the differential current principle to protect line sections of the system. The DC microgrid protection is implemented by blocking and intertripping schemes. However, the use of communication infrastructures for the off-grid LVDC microgrids may lead to high costs. In [16], an adaptive statistical fano factor tool-based protection scheme is proposed to detect and classify faults with enhanced sensor tolerance capability, however, its applicability is demonstrated by simulation results from the PSCAD/EMTDC software. In [17], the OC relay is used to detect low-impedance faults while the wavelet-based protection scheme is proposed to detect high-impedance faults in the microgrid. However, the advanced data collection and processing can make traveling-wave- or artificial-intelligence-based protection methods unsuitable for practical implementation with the possible minimum protection time. In [18], the authors present a handshaking method to detect, locate, and isolate the faulted DC lines. In [19], it depicts differential-current and overcurrent functions with continuous monitoring hardware to detect and isolate the fault without shutting down the entire bus. In [20], the authors propose a protection scheme using the rate of current change and the slope characteristic of the current, but no information about threshold settings of current derivatives. In general, regarding the islanded and small-scaled LVDC microgrids, a fault protection system using local current and voltage measurements with derivative-based tripping thresholds can get a fast fault detection time without paying attention to communication failures, and combined with magnitude-based tripping thresholds to get better adaptability and higher accuracy [21-23].

From the literature review above, this paper proposes a novel statistical and adaptive current and voltage-based fault protection scheme for standalone LVDC microgrids, with main contributions as follows: i) relying on the first-order current and voltage derivatives to quickly detect P2P and P2G faults in a few microseconds right after the fault inception time; ii) improving the adaptability of the protection scheme to the sensor's high noise from local measurements, specifically, a Chi-square-based statistic method is used to adaptively determine tripping thresholds of current and voltage derivatives according to the historical dynamic data of the current and voltage; iii) being adaptable to the directional change of fault currents in the DC microgrid wherein the standard deviation- and mean-based calculation of lower and upper boundaries of the current and voltage is applied for both detection and location of different faults in the system; iv) protecting effectively the source and load branches of the ungrounded/high-impedance-grounded LVDC microgrid based on the over-voltage protection function; and v) validating the proposed fault protection scheme by doing multiple practically staged-fault tests from an off-grid PV-battery-contained LVDC MG testbed instead of using simulation results as in most previous studies.

The structure of the paper is as follows. Section 2 presents a fault analysis of the LVDC microgrid during the standalone operation. More details about the proposed fault protection scheme can be seen in Section 3. In Section 4, the off-grid ungrounded 48Vdc microgrid testbed is described in detail. The microgrid testbed is built to do multiple staged fault tests for validating the suggested protection system. Section 5 presents experimental results; and finally, the main conclusions of this study will be discussed in Section 6.

2. Fault Analysis of the Off-grid LVDC Microgrids

Studying fault current and voltage behaviors of source and energy-storage branches is a significant prerequisite for developing a DC-microgrid protection system [24-26]. A standalone LVDC microgrid network used for fault analysis is shown in Fig. 1. This MG network consists of a PV-source branch, a branch of battery energy storage systems (BESS), and a load branch. In Fig. 1, the symbols of P1, P2, P3, P4, and P5 are protection devices installed to protect PV arrays, PV-boost converters, battery packs, battery converters, and DC loads respectively. Three faulted positions at the DC common bus (F1), the BESS branch (F2), and the load branch (F3) are analyzed in this study. Different fault types of pole-to-pole (P2P), positive-pole-to-ground (PP2G), and negative-pole-to-ground (NP2G)) are also considered during the fault analysis.

2.1. P2P Fault Analysis of Power Converters in Source and Energy-Storage Branches with the Faulted Location F1

In a typical DC microgrid, sources and energy-storage branches are mostly connected to a DC common bus via buck and/or boost converters as shown in Fig. 1. The DC link capacitor of power converters contributes a large fault current in the P2P fault event. Various converter components

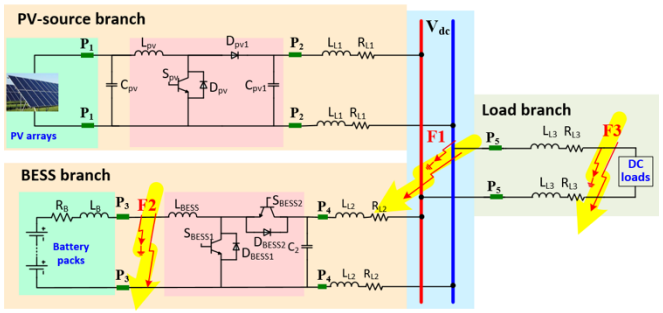

Fig. 1. Network diagram of an off-grid PV-BESS-included LVDC microgrid.

contribute different current values corresponding to fault stages [27]. As seen in Fig. 2 and Fig. 3, for the P2P fault occurrence, non-linear equivalent circuits of the PV-boost converter and BESS bidirectional converter are solved in three distinct time intervals, specifically, the natural response time of the RLC circuit from the fault inception time t_0 to t_1, the response time of the free-wheeling diode from t_1 to t_2, and the time at the steady state from t_2 to onwards.

a) *The natural response stage of the RLC equivalent circuit in the period* $[t_0, t_1)$: All power converters that have the output filter capacitors will go through this stage. From the fault beginning time t_0, the output capacitor begins to discharge through an RLC equivalent circuit, as illustrated in Fig. 2b and Fig. 3b. A second-order differential equation of the RLC circuit can be expressed in the frequency domain by Eq. (1).

$$i_{L,j}(s) = \frac{s v_{C,j}(0)/L_{eq} + i_{L,j}(0)s^2}{s^2 + \frac{R_{ed}}{L_{eq}}s + \frac{1}{L_{eq}C_{eq}}} \tag{1}$$

where $v_{C,j}(0)$ and $i_{L,j}(0)$ are the initial values of the voltage across the output capacitor and the current in the line respectively for the j^{th} power converter right before the fault starting time; "j" = "PV" when considering the PV-boost converter, or "j" = "BESS" when considering the BESS-bidirectional converter, as shown in Fig. 2a and Fig. 3a. The equivalent resistance and inductance of the cable to the faulted location F1 are denoted by R_{eq} and L_{eq}, respectively. In Fig. 1, there are $R_{eq} = 2R_{L1}$, $L_{eq} = 2L_{L1}, C_{eq} = C_{pv1}$ for the PV converter; and $C_{eq} = C_2$ for the BESS converter. In this period $[t_0, t_1)$, the fault current $i_{L,j}(t)\big|_{t_0 \to t_1}$ is significantly contributed by the DC-link capacitor, which can be expressed by Eq. (2) [28].

$$i_{L,j}(t)\big|_{\forall t \in [t_0,t_1)} = \frac{v_{C,j}(0)}{L_{eq}\omega_d}\sin(\omega_d t)e^{-\alpha t} - \frac{i_{L,j}(0)\omega_0}{\omega_d}e^{-\alpha t}\sin\left(\omega_d t - \tan^{-1}\left(\frac{\omega_d t}{\alpha}\right)\right) \tag{2}$$

$$p_1, p_2 = \left(\frac{R_{eq}}{2L_{eq}}\right) \pm \sqrt{\left(\frac{R_{eq}}{2L_{eq}}\right)^2 - \left(\frac{1}{L_{eq}C_{eq}}\right)} \tag{3}$$

$$\begin{cases} p_1, p_2 = \alpha \pm \sqrt{\alpha^2 - \omega_0^2} \\ \omega_d^2 = \alpha^2 - \omega_0^2 \end{cases} \tag{4}$$

According to the value $1/L_{eq}C_{eq}$ that is less than, equal to, or greater than $\left(R_{eq}/2L_{eq}\right)^2$, the values of p_1 & p_2 can be real, imaginary, or complex conjugate, respectively. In case of $p_1 = p_2$, there are $R_{eq} = R_C = 2\sqrt{L_{eq}/C_{eq}}$. The fault current rises at the high rate of *di*/*dt* and gets the peak at the time t_{pk} when the DC-bus voltage reduces to approximately zero.

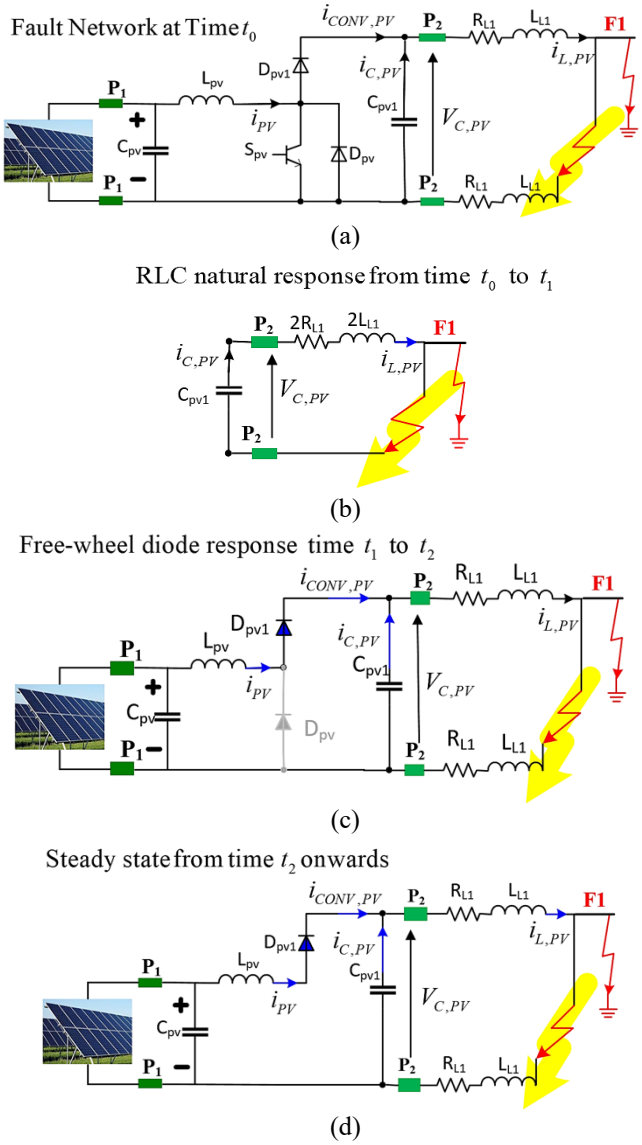

Fig. 2. Fault analysis of the PV-boost converter: (a) faulted converter configuration, (b) RLC equivalent circuit, (c) the free-wheeling diode stage, and (d) the steady state circuit of the converter during the P2P fault at F1.

The peak current magnitude $I_{L,j,pk}$ at the time t_{pk} is expressed as in Eq. (5) and Eq. (6), which depends on fault types, cable parameters, and the DC-bus voltage value $v_{C,j}(t)$.

$$t_{pk} = \frac{1}{\omega_0}\tan^{-1}\left(\frac{\omega_0}{\alpha}\right) \tag{5}$$

$$I_{L,j,pk} \cong \frac{v_{C,j}(0)}{L_{eq}\omega_0} e^{-\alpha t_{pk}} \tag{6}$$

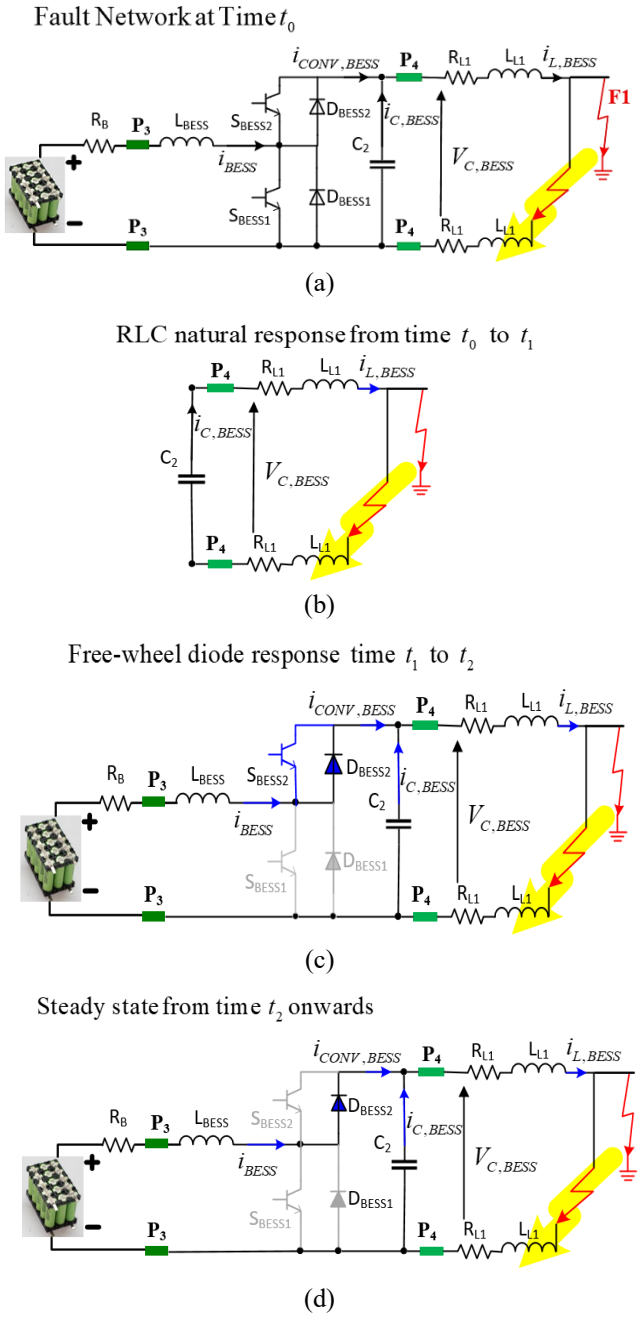

Fig. 3. Fault analysis of the BESS-bidirectional converter: (a) faulted converter configuration, (b) RLC equivalent circuit, (c) the free-wheeling diode phase, and (d) steady state circuit of the converter during the P2P fault at F1.

b) *The free-wheeling diode's conduction stage in the time interval* $[t_1, t_2)$: At this stage, the initial inductor current of power converters begins to contribute its high fault current to the faulted location F1 in the DC microgrid as soon as the voltage of DC-link capacitors drops to a sufficiently low value. As seen in Fig. 2c and Fig. 3c, the high fault current flows through the free-wheel diodes, which may damage the diodes while the controlled switches of converters are turned off to protect themselves. The fault current $i_{L,j}(t)\big|_{t_1 \to t_2}$ at this second stage is expressed by Eq. (7).

$$i_{L,j}(t)\big|_{t_1 \to t_2} = i'_{L,j}(0)e^{-(R_{eq}/L_{eq})t}, \forall t \in [t_1, t_2) \tag{7}$$

$$i_{L,j}(t)\big|_{t_1 \to t_2} = i_{CONV,j}(t) + i_{C,j}(t), \forall t \in [t_1, t_2)$$
$$i_{C,j}(t) \to 0; \text{ with "}j\text{" = "PV" or "BESS"} \tag{8}$$

where the initial line/cable current at the converter output with the starting time t_1 is denoted by $i'_{L,j}(0)$. This stage contains the converter's free-wheel diodes with high fault current contributions and therefore must be taken into account when designing a DC-microgrid protection system. It has been investigated that the critical time t_{pk} of the peak current is when the power converter enters the free-wheeling stage. The expected protection time t_{op} is expressed in Eq. (9), which includes the detection time and the fault clearing time.

$$t_{op} + t_{cb} + t_{com} \le t_{pk} \to t_{op} \le t_{pk} - t_{cb} - t_{com} \tag{9}$$

where the communication delay is denoted by t_{com} and the working/switching time of circuit breakers (or solid-state relays) is denoted by t_{cb}.

c) *The steady-state fault stage from the time* t_2 *onwards*: If the power converter operates as the buck converter, it will not contribute any current if the P2P fault persists for a long period, or longer than the time t_2. However, in the case of boost converters and bidirectional DC-DC converters, there are current-source responses forced by the cable inductor and the DC-link capacitor in the converters. As illustrated in Fig. 2d, the controlled switches of the converters are blocked, at this steady-state stage the fault current of the PV-boost converter, $i_{L,PV}(t)$, contributed by the PV source can be obtained, as expressed in Eq. (10) and Eq. (11).

$$i_{L,PV}(t)\big|_{t_2 \to \infty} = i_{SC,PV}(t), \forall t \ge t_2 \tag{10}$$

$$i_{SC,PV}(t) = \left(I_{SC,STC} + K_i(T - T_{STC})\right)\left(\frac{G}{G_{STC}}\right) \tag{11}$$

where K_i is a current temperature coefficient for the photo-current, normally at 3~5mA/°C [29]; G_{STC} and T_{STC} are the solar irradiance and ambient temperature at the standard test condition (STC), i.e. 1000 W/m^2 and

25°C, respectively; G and T represent non-standard quantities under random changes in solar irradiance and temperature; and $I_{SC,STC}$ is the short-circuit current of the PV source at the STC. As seen in Fig. 3d, the fault current, $i_{L,BESS}(t)$, in the time domain contributed by the battery source in the BESS branch can be expressed as in Eq. (12).

$$i_{L,BESS}(t)\Big|_{\forall t\geq t_2} = \frac{v_{batt}}{R_{eq}+R_B}\left(1-e^{-t/\tau_{batt}}\sin(\omega_d t)\right) \quad (12)$$

where L_{BESS} is the inductance of the BESS-bidirectional converter and $\tau_{batt} = (L_{BESS}+2L_{L1})/(R_{eq}+R_B)$; and R_B is the internal resistance of the battery source.

2.2. P2P Fault Analysis of Battery and Load Branches Corresponding with the Faulted Locations F2 and F3

When a P2P fault occurs at the load branch (i.e. a faulted position at F3) in the LVDC microgrid, fault responses of the PV-source branch and the BESS branch are similar to their responses in the case of the faulted location F1. However, it is necessary to consider further line resistance and inductance, R_{L3} and L_{L3}, as seen in Fig. 1, which will significantly affect the exponential damping coefficient, the natural and resonant frequencies, and the arbitrary constant of the equivalent fault circuit diagram of the DC microgrid. In addition, when a P2P fault happens at the terminal of battery packs (i.e. a faulted position F2) as shown in Fig. 1, the battery fault current, $i_{Bat}(t)$, is calculated by Eq. (13) [30].

$$i_{Bat}(t) = \frac{v_{Bat}(0)}{R_B}\left(1-e^{-t\left(\frac{R_B}{L_B}\right)}\right) \quad (13)$$

where R_B and L_B are the internal resistance and inductance of the battery source, respectively; and $v_{Bat}(0)$ is the battery's initial operating voltage just before the fault occurrence. Protection devices, P3, as fast-acting DC fuses are commonly used to protect the battery packs in the system.

2.3. P2G Fault Analysis of Power Converters in Source and Energy-Storage Branches with the Faulted Locations F1, F2, and F3

A standalone and small-sized low-voltage DC microgrid is mostly ungrounded or high-impedance grounded, so if a pole-to-ground (P2G) fault occurs at F1, F2, or F3 in the DC microgrid as seen in Fig. 1, the P2G fault current is considered as the DC leakage current which may insignificantly affect the continuous operation of the MG. In general, it is possible to identify the negative/positive-pole-to-ground faults based on over-voltage characteristics or the rate of change of voltage at the positive or negative line of the DC microgrid. It is possible to sample the voltages at the positive and negative poles of the LVDC microgrid by creating a middle point of two series-connected capacitors at the DC bus in order to get the common voltage. Hence, the positive-pole voltage is the potential difference between the (+) pole and the middle point of the DC-link capacitors, while the negative-pole voltage is the potential difference between the (-) pole and this middle point in the DC microgrid configuration.

3. A Statistical and Adaptive Current and Voltage-Based Fault Protection System for DC Microgrids

A flowchart of the novel statistical and adaptive current and voltage-based fault protection system for islanded LVDC microgrids is shown in Fig. 4. There are four main stages of the protection scheme, including i) the stage of sampling and abnormal operation detection; ii) the stage of only P2P fault detection; iii) the stage of P2P fault detection and identifying the direction change of fault current; and iv) the stage of P2G fault detection in the protection system.

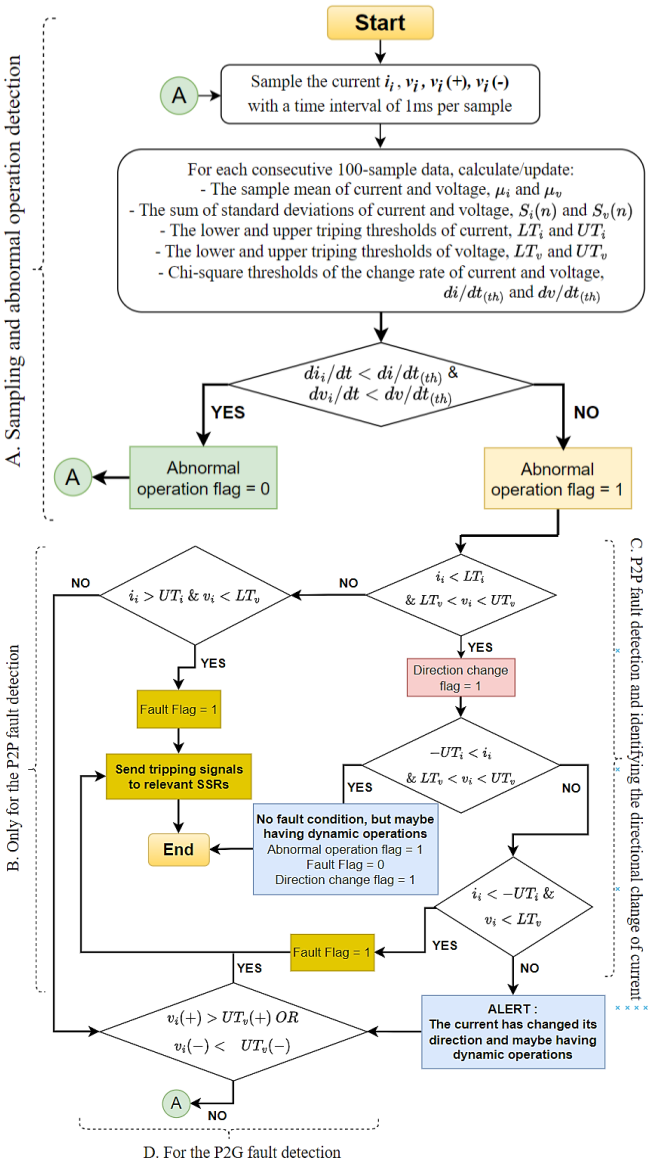

Fig. 4. A flow chart of the statistical and adaptive current and voltage-based fault protection system proposed for the islanded LVDC microgrids.

In addition, the developed DC-microgrid protection uses solid-state relays (SSR) to clear the fault right after the proposed protection scheme sends tripping signals to them. Solid-state relays are equipped with microcontrollers to set up their tripping thresholds. The switching time of SSRs is normally about 50μs ~ 100μs. The current and voltage can be locally measured by current and voltage transducers with a time interval of one millisecond per sample.

3.1. Parameter/Threshold Settings for the Proposed DC-Microgrid Protection System

At the first stage (Stage A as seen in Fig. 4), the current parameter, i_i, the voltage between positive (+) and negative (-) poles, v_i, the positive voltage between the (+) pole and the common point, $v_i(+)$, and the negative voltage between the (-) pole and the common point, $v_i(-)$, are sampled at the time interval of one millisecond in the LVDC microgrid, where the subscript "i" is the order number of samples. For each consecutive 100-sample data of the above signals, the proposed DC-microgrid protection system will calculate the thresholds of μ_i, μ_v, $\mu_{v(+)}$, $\mu_{v(-)}$, $S_i(n)$, $S_v(n)$, LT_i, UT_i, LT_v, UT_v, $UT_v(+)$, $UT_v(-)$, $di/dt_{(th)}$, and $dv/dt_{(th)}$ as shown in the following equations.

In this study, the sample mean calculation of currents and voltages, μ_i, μ_v, $\mu_{v(+)}$, and $\mu_{v(-)}$ for each consecutive 100-sample data is expressed in Eq. (14). The sum of standard deviations of current and voltage $S_i(n)$ and $S_v(n)$ can be calculated by Eq. (15) and Eq. (16). The lower and upper tripping thresholds of the current, LT_i and UT_i, can be determined by Eq. (17) and Eq. (18). The lower and upper tripping thresholds of the voltage LT_v and UT_v can be determined by Eq. (19) and Eq. (20).

$$\begin{cases} \mu_i = \dfrac{i_{i-99} + \ldots + i_i}{100} \\ \mu_v = \dfrac{v_{i-99} + \ldots + v_i}{100} \\ \mu_{v(+)} = \dfrac{v_{i-99}(+) + \ldots + v_i(+)}{100} \\ \mu_{v(-)} = \dfrac{v_{i-99}(-) + \ldots + v_i(-)}{100} \end{cases} \quad (14)$$

$$S_i(n) = \sum_{j=i-99}^{i} \left(i_j - \mu_i\right) \quad (15)$$

$$S_v(n) = \sum_{j=i-99}^{i} \left(v_j - \mu_v\right) \quad (16)$$

$$LT_i = \mu_i - k * sqrt\left(\frac{(S_i(n))^2}{100}\right) \quad (17)$$

$$UT_i = \mu_i + k * sqrt\left(\frac{(S_i(n))^2}{100}\right) \quad (18)$$

$$LT_v = 0.5 * \mu_v \quad (19)$$

$$UT_v = 1.5 * \mu_v \quad (20)$$

According to the overvoltage characteristic for the P2G fault in the un-grounded or high-impedance grounded LVDC microgrid, the upper thresholds of the voltage between the (+) pole and the common point, $UT_v(+)$, and the voltage between the (-) pole and the common point, $UT_v(-)$, are calculated by Eq. (21) and Eq. (22), where an empirical factor of k_e is selected in a reliable range of 1.2 ~ 1.5.

In addition, to improve the adaptability of the proposed protection scheme regarding the sensor's high noise of local measurements, a Chi-square-based statistic method is proposed to determine tripping thresholds of current and voltage derivatives, $di/dt_{(th)}$ and $dv/dt_{(th)}$. For the one-sided confidence interval of the current derivative di/dt (or the voltage derivative dv/dt), Chi-square thresholds of the current derivative $\chi^2\{di/dt\}_{n-1,1-\alpha} = di/dt_{(th)}$ (and the voltage derivative $\chi^2\{dv/dt\}_{n-1,1-\alpha} = dv/dt_{(th)}$) can be expressed by Eq. (23) and Eq. (24), where n is the total number of samples used for the Chi-square distribution, selected to 100 samples and $(1-\alpha)$ is the confidence coefficient, selected to 95%. $\sigma\{di/dt\}_{n,1-\alpha}$ and $\sigma\{dv/dt\}_{n,1-\alpha}$ are the standard deviations of the random variables di/dt and dv/dt, which are the positive square root of variances of $\sigma^2\{di/dt\}_{n,1-\alpha}$ and $\sigma^2\{dv/dt\}_{n,1-\alpha}$ with the Chi-square-based confidence coefficient (1-α), respectively; $Z_{N\left(\mu_{di/dt},\sigma^2\right)}$ and $Z_{N\left(\mu_{dv/dt},\sigma^2\right)}$ are the constant values obtained from the standard normal distribution table with the selected confidence level (1-α).

$$UT_v(+) = k_e * \mu_{v(+)} \quad (21)$$

$$UT_v(-) = k_e * \mu_{v(-)} \quad (22)$$

$$di/dt_{(th)} = \mu_{di/dt} + Z_{N\left(\mu_{di/dt},\sigma^2\right)}\left(\sigma\{di/dt\}_{n,1-\alpha}\right) \quad (23)$$

$$dv/dt_{(th)} = \mu_{dv/dt} + Z_{N\left(\mu_{dv/dt},\sigma^2\right)}\left(\sigma\{dv/dt\}_{n,1-\alpha}\right) \quad (24)$$

$$\frac{di_i}{dt} = \frac{i_i - i_{i-1}}{\Delta t};\ \frac{dv_i}{dt} = \frac{v_i - v_{i-1}}{\Delta t},\ \text{with } \Delta t = 0.001s \quad (25)$$

$$\mu_{di/dt} = \sum_{j=i-99}^{i}\left(\frac{di_j}{dt}\right)\Big/100\ ;\ \mu_{dv/dt} = \sum_{j=i-99}^{i}\left(\frac{dv_j}{dt}\right)\Big/100 \quad (26)$$

$$\sigma^2\{di/dt\}_{n,1-\alpha} \in \left[\sum_{i=1}^{n}\left(\left(di_i/dt - \mu_{di/dt}\right)^2\Big/\chi^2\{di/dt\}_{n-1,1-\alpha}\right), \infty\right) \quad (27)$$

$$\sigma^2\{dv/dt\}_{n,1-\alpha} \in \left[\sum_{i=1}^{n}\left(\left(dv_i/dt-\mu_{dv/dt}\right)^2 \Big/ \chi^2\{dv/dt\}_{n-1,1-\alpha}\right),\infty\right] \quad (28)$$

3.2. Pole-to-Pole Fault Detection in the LVDC Microgrid

Right after completing threshold determination in the developed DC-microgrid protection scheme, the conditions $di_i/dt < di/dt_{(th)}$ and $dv_i/dt < dv/dt_{(th)}$ are checked. If all two conditions are correct, the operation of the microgrid system is normal (i.e. the flag of the abnormal operation is "0"). Otherwise, if one of the two conditions is incorrect, then the system operation is at an abnormal state (i.e. the flag of the abnormal operation is "1"), as presented in Stage A of the proposed protection system.

Next, two conditions $i_i < LT_i$ and $LT_v < v_i < UT_v$ are checked, if they are correct, one can conclude that the fault current direction in the microgrid has been changed (i.e. the direction change flag is "1"). Then, two conditions $-UT_i < i_i$ and $LT_v < v_i < UT_v$ are next evaluated, if they are right, one can conclude that there is no faulted condition in the DC microgrid (i.e. the fault flag is "0"), but there may be other dynamic operations in the system; otherwise, two following conditions $i_i < -UT_i$ and $v_i < LT_v$ are afterward estimated, if they are correct, one can conclude that the direct/low-impedance P2P fault has occurred in the DC microgrid (i.e. the fault flag is "1"), hence, tripping signals will be sent to the relevant SSRs to clear the P2P fault. However, if the two conditions $i_i < -UT_i$ and $v_i < LT_v$ are wrong, one can only conclude/alert that the current has changed its direction, and one of dynamic operations such as the load-power change, the source-power change, may have happened in the microgrid, as indicated by Stage C of the protection algorithm in Fig. 4. After that, the proposed protection will continue to detect the P2G fault in the MG as mentioned in Section 3.3.

On the other hand, if the two conditions $i_i < LT_i$ and $LT_v < v_i < UT_v$ are non-satisfied, two following constraints $i_i > UT_i$ and $v_i < LT_v$ are checked then. If both $i_i > UT_i$ and $v_i < LT_v$ are correct, one can state that the direct/low-impedance P2P fault has occurred in the microgrid (i.e. the fault flag is "1") and there is no change in the fault current direction; hence, tripping signals will be sent to the relevant SSRs to clear the P2P fault, as indicated in Stage B of the protection algorithm in Fig. 4. Nevertheless, if $i_i > UT_i$ and $v_i < LT_v$ are incorrect, the proposed protection will continue to detect the P2G fault events as mentioned in Section 3.3.

3.3. Pole-to-Ground Fault Detection in the LVDC Microgrid

As shown in Fig. 4, if the two conditions of $i_i < -UT_i$ and $v_i < LT_v$ are all wrong or the constraints of $i_i > UT_i$ and $v_i < LT_v$ are also all incorrect, then the proposed fault protection scheme will check the two following conditions of $v_i(+) > UT_v(+)$ & $v_i(-) < UT_v(-)$. If one of these two conditions is satisfied, it can be concluded that the P2G fault has occurred in the ungrounded or high-impedance grounded LVDC microgrid, as indicated at Stage D of the protection algorithm. Hence, tripping signals will be sent to the relevant SSRs to clear the P2G fault event in the system. Otherwise, the protection procedure will be repeated from point A of the flowchart as described in Fig. 4.

4. An Off-grid PV-Battery-based Low-Voltage DC Microgrid Testbed and Multiple Staged Fault Tests

To demonstrate the effectiveness of the statistical and adaptive current and voltage-based fault protection system for islanded LVDC microgrids, the staged tests of P2P, positive-pole-to-ground (PP2G), negative-pole-to-ground (NP2G) faults are implemented at the common DC-bus (F1), as shown in Fig. 5. Many serious P2P faults with the zero fault-impedance (i.e. the direct short-circuit faults) are studied. The PP2G/NP2G faults are high-impedance faults because this off-grid LVDC MG testbed is ungrounded. Microcontrollers TM4C are used to run the proposed fault protection program, as seen in Fig. 6.

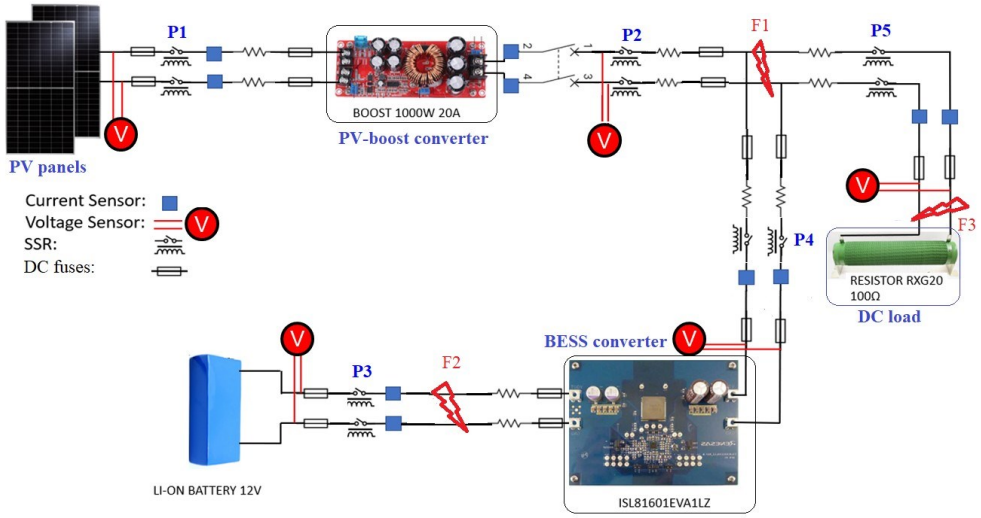

Fig. 5. An off-grid PV-Battery-based LVDC microgrid testbed.

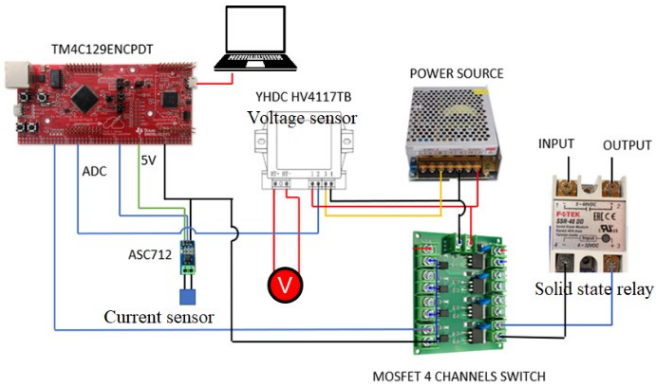

Fig. 6. Control circuit of SSRs from the proposed DC-microgrid protection scheme.

The standalone 48Vdc MG testbed consists of i) two parallel-connected solar panels with an operating voltage of 40.5V, a rated-current value of about 3.52A, a short-circuit current of 4.86A, and a rated power of about 80W at standard testing conditions; ii) fast-acting DC fuses; iii) solid-state relays and their activation circuits installed at positions of P1, P2, P3, P4, and P5 in the system; iv) current and voltage transducers; v) an adjustable 12~80Vdc PV boost converter rated at the power 1000W and the current 20A; vi) a 150W & 48V-12V bidirectional BESS converter; vii) 12V Li-ion battery packs; and viii) DC loads. Line resistance is 20mΩ per km, line inductance is 100μH per km, and the filter capacitor is 25 mF.

5. Experimental Results of the Statistical and Adaptive Current and Voltage-Based Fault Protection Scheme for a LVDC Microgrid Testbed

5.1. Protection Results of the Algorithm Regarding the P2P Faults at F1, F2 & F3 in the DC MG Testbed

a) *P2P faults at the common bus (F1)*: When a direct pole-to-pole fault occurs at the DC common bus (F1), the proposed protection system can detect and clear the fault very fast in a few milliseconds to protect the PV-source branch and the BESS branch in the DC MG, as shown in Fig. 7, Fig. 8, and Fig. 9. Noted that the time interval between two adjacent samples is one millisecond. For more detailed, Fig. 7 shows the protection results of the PV-source branch. Lower and upper thresholds $[LT_i, UT_i]$ of the current at the PV-source branch are 1.1A to 1.7A. Similarly, thresholds of $[-LT_i, -UT_i]$ are approximately -1.1A to -1.7A. Tripping thresholds LT_v and UT_v are calculated to be 28.5V and 60.5V respectively. It is noted that these thresholds are updated for each consecutive 100-sample data of current and voltage signals in the system. When a direct P2P fault F1 occurs, both the current and voltage at the output of the PV-boost converter experience a steep change in value in a very short amount of time, specifically the peak fault current at around 3.5A and the voltage drops from 48 volts to under 5 volts. Therefore, two constraints $i_i > UT_i$ and $v_i < LT_v$ are satisfied, and the tripping signal is sent to the SSR at position P2 to clear the P2P fault at F1. The fault protection time of the system for the PV-source branch is about 3ms.

Fig. 8 and Fig. 9 show the protection results of the BESS branch for the direct P2P fault at F1 when the BESS is charging or discharging respectively. In case of the charging state of the BESS, as indicated in Fig. 8, the branch current changes its direction when the fault happens at F1. The fault current i_i is larger than both $-LT_i$ and UT_i, so the directional change of current has occurred at the BESS branch. Moreover, the voltage at the output of the BESS converter significantly reduces below its lower tripping. Therefore, the two conditions $i_i > UT_i$ and $v_i < LT_v$ are satisfied, consequently, the direct P2P fault at F1 is detected and isolated to protect the battery branch in the MG with the actual fault protection time of about 5ms. In case of the discharging state of the BESS, as presented in Fig. 9, the branch current does not change its direction but exceeds the upper tripping threshold, so the tripping signal is sent to the SSR at position P4 to isolate the fault with the total fault cleating time of about 3ms.

Table 1 summarises the achieved experimental results of the proposed DC-microgrid protection scheme with regard to the P2P fault event at F1 and also shows detailed discussions of this protection scheme. Noted that the faulted position F1 is the most serious fault occurrence of the DC MG because it is at the DC-common bus wherein all source and energy-storage branches are mostly susceptible with this P2P fault type. Regardless of large transients and measurement noises of the current and voltage during the standalone operation of the $48V_{dc}$ DC microgrid testbed, the direct/low-impedance P2P fault at the common bus can be detected and cleared within a few milliseconds.

b) *P2P faults at the battery's terminal (F2) and the load branch (F3) in the LVDC microgrid testbed*: In case of the P2P fault occurring at the battery's terminal (F2), the switching devices of BESS-bidirectional converter are quickly blocked to protect themselves from the high fault current flowing from the DC common bus into the faulted position. The protective device, a solid-state relay, at the position P3, is used to protect the battery against the fault.

As shown in Fig. 10, regarding the seriously direct/low-impedance P2P fault at F2, the fault is detected at about 3ms after the fault inception. With the low-impedance P2P fault at the battery, though the battery fault current gets high within a short time and also exceeds its upper tripping threshold, the battery fault voltage might only gradually reduce if the battery capacity is full right before the fault occurrence. Hence, an abnormal operation alert of the battery can be quickly given by the proposed protection system regarding the low-impedance P2P fault at F2, i.e. the flag of the abnormal operation of the algorithm is "1", but the fault detection time can be a little bit longer. Furthermore, it can be suggested to use the additional fast-acting DC fuses for the proposed algorithm to protect the battery more reliably.

When a direct P2P fault happens at the load branch (F3), the protective device, a solid-state relay, at the position P5 must be activated to clear the fault. The total fault current is contributed by both the PV-source and BESS branches in the system. As indicated in Fig. 11, the load fault current increases quickly from 0.6A up to 8.0A, so the condition $i_i > UT_i$ is satisfied. In addition, the load fault voltage experiences a steep

drop from 48 volts down to unstable 14 volts and finally 7 volts, so the condition $v_i < LT_v$ is also satisfied. Consequently, according to two constraints at Stage B of the proposed algorithm, the P2P fault at F3 is rapidly detected within 2ms. The SSR at the position P5 can be very fast activated in some microseconds to clear the fault. Table 2 summarises the achieved experimental results of the proposed DC-microgrid protection scheme with regard to the direct/low-impedance P2P fault events at F2 and F3 and gives detailed discussions of this protection scheme. Noted that the staged fault test at F2 is to validate the protection scheme for protecting the battery storage device, while the staged fault test at F3 is to check the suggested protection operation for protecting the load branch in the DC microgrid.

Table 1. Summary and discussion on the achieved experimental results of the proposed protection scheme with regard to the P2P fault event at F1 in the DC-microgrid testbed

Protection cases	**Pole-to-pole fault at the common DC-bus F1 of the off-grid 48V$_{dc}$ MG testbed**	
	The fault-clearing time	***Discussions***
Protection results of the PV-source branch	3ms	When the P2P fault occurs at the common bus, the DC-link capacitor of the PV boost converter discharges very fast to the faulted position F1, therefore, the change of the current with respect to time is very high and right after the two constraints $i_i > UT_i$ and $v_i < LT_v$ are also satisfied; consequently, the SSR at the position P2 as indicated in Fig. 5 is very quickly activated to isolate the faulted position F1 and to protect the PV-source branch within the expected time of 3ms. By comparing the methods presented in [31-33], the proposed protection scheme is superior to protect the PV-source branch from the P2P fault occurrence in the DC microgrid system.
Protection results of the BESS branch under the charging operation mode	5ms	In this study, the charging current is negative while the discharging current is positive as seen in Fig. 8 ang Fig. 9 respectively. Irrespective of the charging and discharging operation modes of the BESS branch, the proposed protection scheme can detect and clear very fast the P2P fault occurrence at the common bus. The output capacitor of the battery bidirectional converter contributes a high fault current to the faulty location F1, so not only the *di*/*dt* value is very high but also two constraints $i_i > UT_i$ and $v_i < LT_v$ are correct; as a result, the SSR at the position P4 is activated to protect the BESS branch from the P2P fault F1 within 3 ~ 5ms right after the fault inception.
Protection results of the BESS branch under the discharging operation mode	3ms	

Table 2. Summary and discussion on the achieved experimental results of the proposed protection scheme with regard to the P2P fault events at F2 and F3 in the DC-microgrid testbed

Protection cases	**Pole-to-pole fault at the battery's terminal (F2) and the load branch (F3) of the off-grid 48V$_{dc}$ microgrid testbed**	
	The fault-clearing time	***Discussions***
Protection results of the battery source from the P2P fault at F2	3ms	• It is proposed to combine the developed DC-microgrid protection scheme with fast-acting fuses to protect the battery packs when the P2P fault occurs at F2. These fuses work as the back-up protection for the SSR in the studied microgrid [34]. • The change in battery fault current is very high such that the SSR at the position P3 can be quickly activated to protect the battery packs. • This study does not consider the inside protection of BESS-bidirectional converter because these switching devices of the converter will be rapidly blocked to protect themselves from the short-circuit occurrence [35]. • By comparing the methods presented in [31-33], the proposed protection scheme is superior to protect the battery packs from the P2P fault at F2.
Protection results of the load branch from the P2P fault at F3	2ms	• Solid-state relays at the positions P2, P4, and P5 in the DC MG testbed can accurately detect the P2P fault event at F3 because of the very high current change and satisfaction of both the conditions $i_i > UT_i$ and $v_i < LT_v$ at Stage B of the protection algorithm. • The tripping operation of P2, P4 and P5 are determined by a coordination time interval of 5ms. In case all the devices P2, P4 and P5 simultaneously find out the fault event at F3, the relay P5 will be firstly activated to protect the load branch. If the P2P fault F3 still remains until 5ms after the fault inception time, the relays P2 & P4 will be next activated to clear this fault. This time interval-based protection coordination is suitable with the off-grid and small-scaled LVDC MG instead of using the communication links to coordinate among the devices P2, P4 & P5 as presented in [15, 36].

5.2. Protection Results of the Algorithm Regarding Pole-to-Ground Faults at F1 in the DC MG Testbed

When a positive-pole-to-ground (PP2G) fault occurs at the common bus (F1), the fault voltage responses of the PV-source and BESS branches are shown in Fig. 12 and Fig. 13 respectively. The proposed protection scheme will check two conditions $v_i(+) > UT_v(+)$ and $v_i(-) < UT_v(-)$, if one of them is correct, then the algorithm can detect the high-impedance PP2G fault in the ungrounded 48V$_{dc}$ DC microgrid testbed. Just after the fault occurrence, the voltage value $v_i(-)$ decreases to approximately -47V lower than the threshold $UT_v(-)$ of about -27V. Therefore, the fault can be identified within 3ms by the suggested protection algorithm.

In addition, Fig. 14 and Fig. 15 also show tripping thresholds and fault voltage waveforms at the PV-source and BESS branches for the NP2G fault at F1. The voltage value $v_i(+)$ increases to approximately $+47$V higher than the tripping threshold $UT_v(+)$ of about $+29$V. Therefore, the NP2G fault can also be identified within 3ms by the suggested protection algorithm. One can conclude that the statistical and adaptive current and voltage-based fault protection system is effective and validated for detecting high-impedance faults in off-grid ungrounded or high-impedance-grounded low-voltage DC microgrids.

Table 3 summarises the achieved experimental results of the proposed DC-microgrid protection scheme with regard to PP2G and NP2G fault events at F1 and shows detailed discussions of this protection scheme. Noted that the off-grid 48V$_{dc}$ MG testbed is ungrounded. The SSRs at the positions P2 and P4 should detect high impedance faults in the DC microgrid based on the over-voltage protection function as presented in most previous studies [5, 7, 17, 36].

Table 3. Summary and discussion on the achieved experimental results of the proposed protection scheme with regard to the PP2G and NP2G fault events at F1 in the DC-microgrid testbed

Protection cases	**Positive/negative pole-to-ground faults at the common DC-bus F1 of the off-grid 48V$_{dc}$ MG testbed**	
	The fault-clearing time	***Discussions***
Protection results of the PV-source branch and the BESS branch for the PP2G fault at F1	3ms	• The proposed DC-microgrid protection can effectively work to protect the source and load branches of the ungrounded/high-impedance-grounded microgrid based on the overvoltage response of negative and positive lines. • In case of different P2G faults, the protection algorithm can send a tripping signal to the relevant SSR to clear the fault or give an abnormal operation alert of the MG regarding high-impedance faults. • The empirical-factor- and sample-mean-based calculation of lower and upper boundaries of the voltage, $UT_v(+)$ and $UT_v(-)$, as shown in Eq. (21) and Eq. (22), is effectively applied for identifying different high-impedance faults in the DC-microgrid system. • The proposed protection scheme is validated by the practical staged-fault testing results from an off-grid PV-battery-contained 48V$_{dc}$ MG testbed instead of the simulation results.
Protection results of the PV-source branch and the BESS branch for the NP2G fault at F1	3ms	

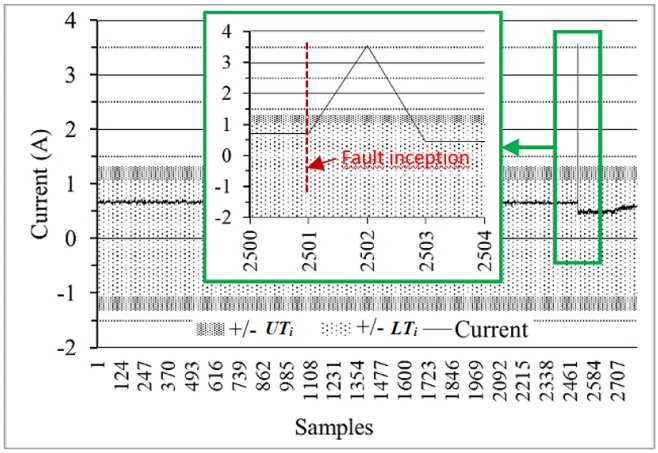

(a) Fault current waveform at the output of the PV-source branch.

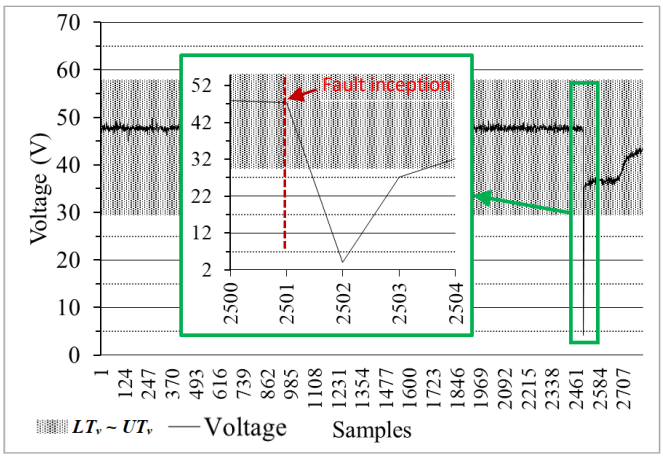

(b) Fault voltage waveform at the output of the PV-source branch.

Fig. 7. Protection results of the PV-source branch for the direct P2P fault at the DC common bus F1.

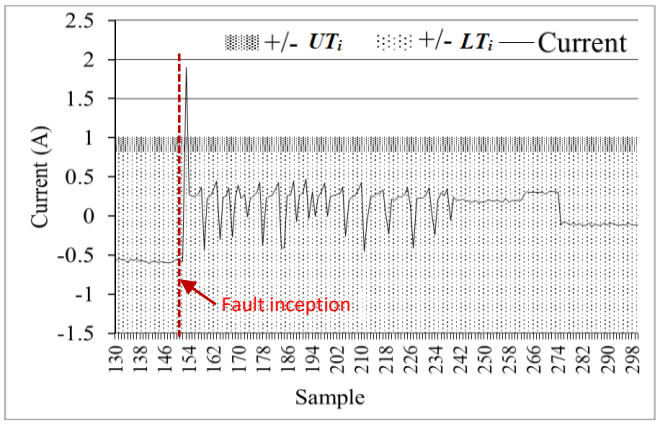

(a) Fault current waveform at the output of the BESS branch.

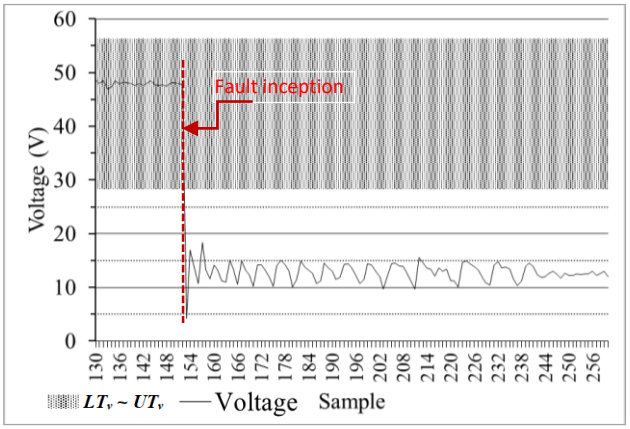

(b) Fault voltage waveform at the output of the BESS branch.

Fig. 8. Protection results of the BESS branch for the direct P2P fault at the DC common bus (F1) when the BESS is under the charging operation.

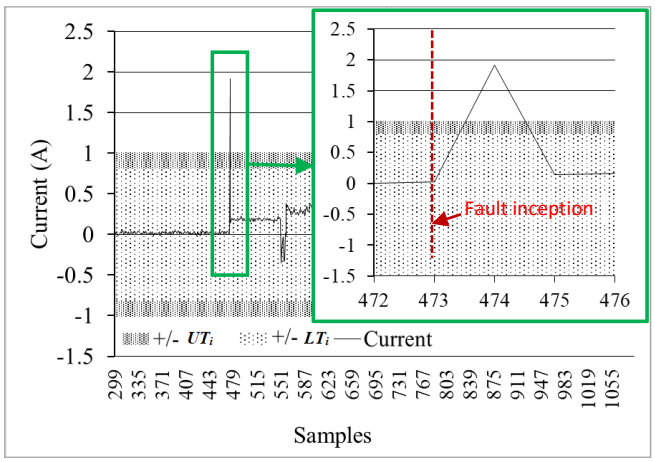

(a) Fault current waveform at the output of the BESS branch.

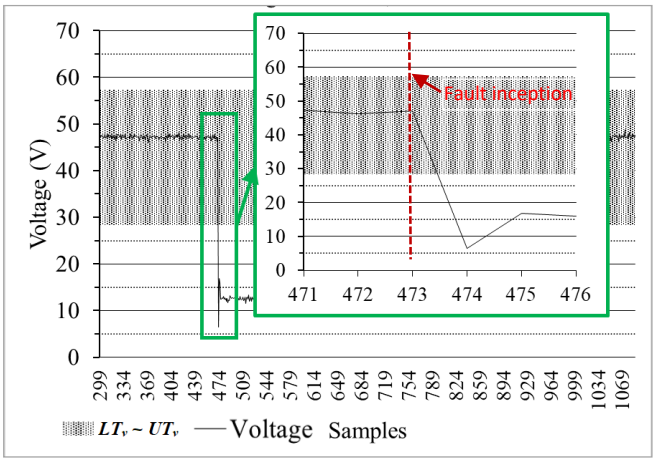

(b) Fault voltage waveform at the output of the BESS branch.

Fig. 9. Protection results of the BESS branch for the direct P2P fault at the DC common bus (F1) when the BESS is under the discharging operation.

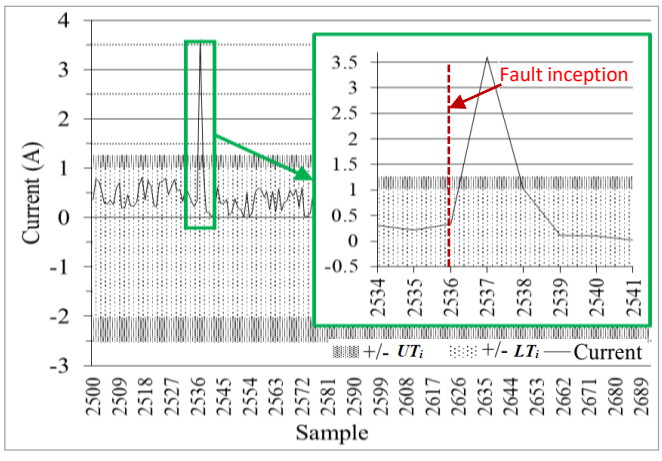

(a) Fault current waveform at the battery output.

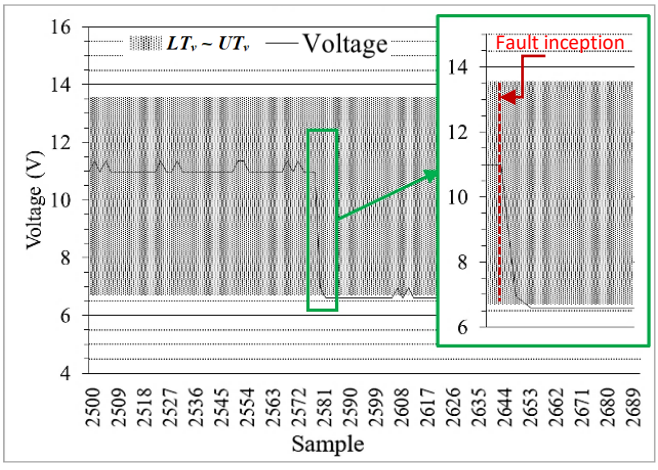

(b) Fault voltage waveform at the battery output.

Fig. 10. Protection results of the battery packs for the direct P2P fault at F2 when the BESS is discharging.

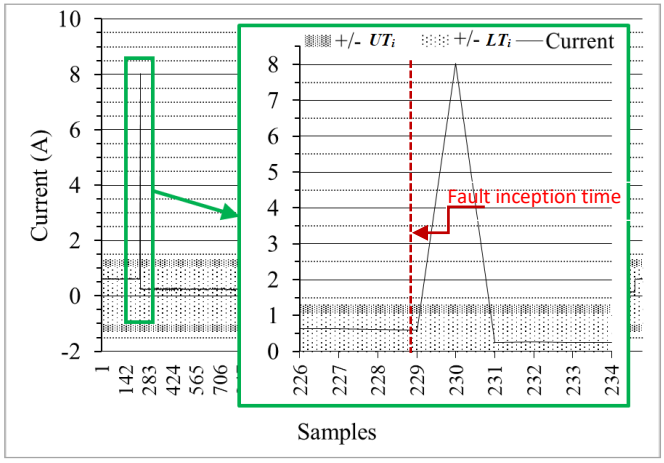

(a) Fault current at the load branch in the 48V_{dc} microgrid testbed.

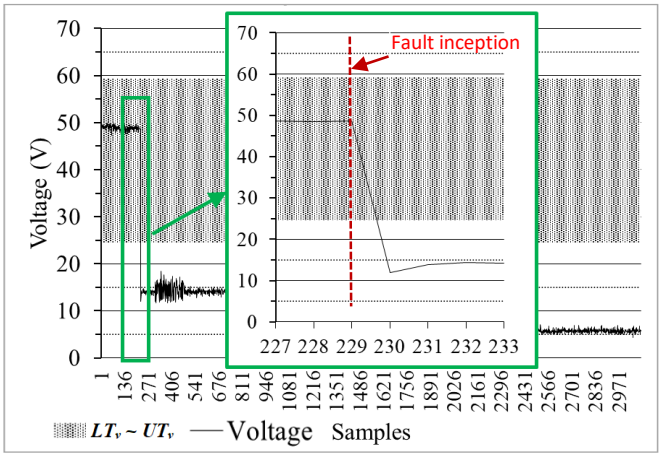

(b) Fault voltage waveform at the load branch in the MG testbed.

Fig. 11. Protection results of the load branch in the 48V_{dc} MG testbed for the direct P2P fault at F3.

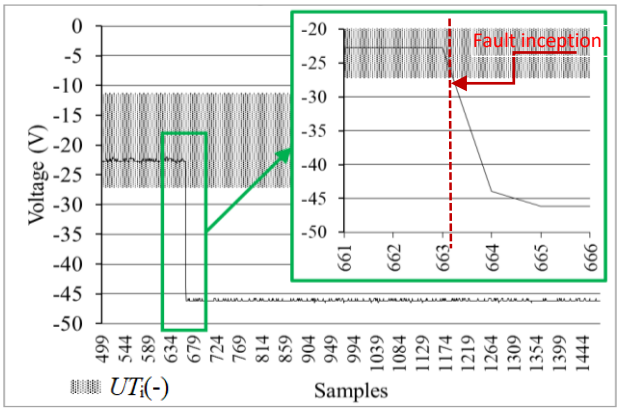

Fig. 12. Tripping thresholds and fault voltage waveform at the PV-source branch for the PP2G fault at F1.

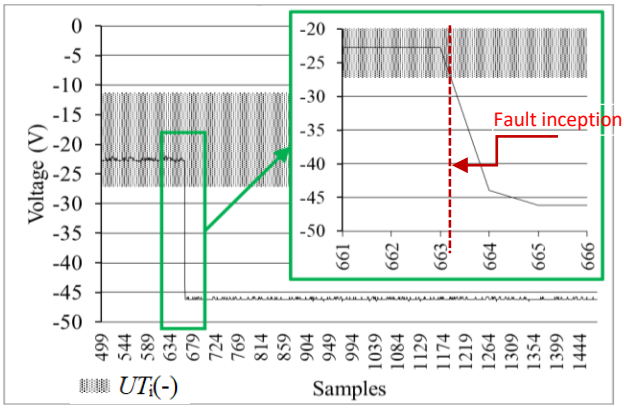

Fig. 13. Tripping thresholds and fault voltage waveform at the BESS branch for the PP2G fault at F1.

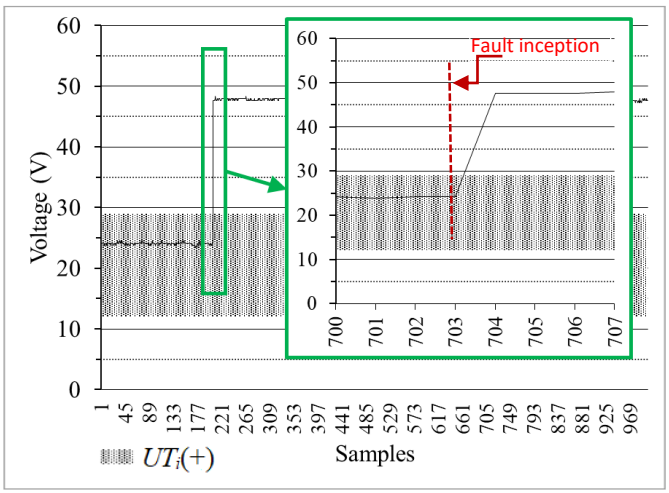

Fig. 14. Tripping thresholds and fault voltage waveform at the PV-source branch for the NP2G fault at F1.

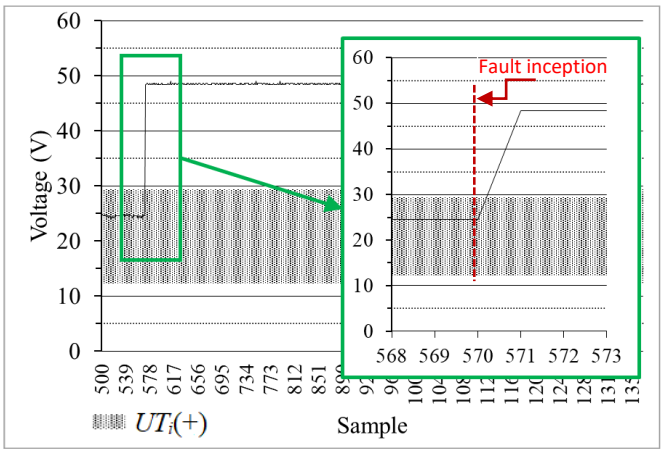

Fig. 15. Tripping thresholds and fault voltage waveform at the BESS branch for the NP2G fault at F1.

6. Conclusions

This paper has developed a novel statistical and adaptive current and voltage-based fault protection scheme for ungrounded/high-impedance-grounded standalone low-voltage DC microgrids. This developed microgrid protection can quickly detect the P2P and P2G faults within a few microseconds of the inception time. Chi-square-based tripping thresholds of the first-order current and voltage derivatives are effectively used for the proposed protection algorithm to adapt to the sensor's high noise of local current and voltage measurements in the LVDC microgrid. Tripping thresholds of

the protection can be continuously updated for each pre-determined sampling data package from the measurement system. The standard deviation- and mean-based calculation of lower and upper boundaries of current and voltage are properly applied for the protection algorithm to get high adaptability with the directional change of fault currents in the PV-battery-based DC microgrid. Experimental results of staged fault tests from the islanded 48V_{dc} microgrid testbed have been presented and analysed in this study to demonstrate the effectiveness of the proposed algorithm for protecting the PV-source, energy-storage, and load branches of the ungrounded/high-impedance-grounded and small-scaled

device/package to integrate the microcontroller with the

solid-state DC circuit breaker, which will be then tested under different configurations and operation modes of the DC-microgrid (e.g. DC microgrids with the effective grounding system, the larger power capability, the higher operating voltage, the integration of more PV sources or more energy-storage devices, or with the grid-connected operation mode).

Acknowledgements

The authors would like to acknowledge to Mr. Huynh Thanh Tung, Mr. Dinh Trinh Minh Khoi, and Mr. Le Hoang Khang at Vietnamese-German University (VGU) for their support to do staged fault tests of the DC-microgrid testbed in this study. This work was also supported and funded by Vietnamese-German University with a decision number of 677/QĐ-ĐHVĐ and a project code of DTCS-2023-003.

Author Contributions

D. M. Bui was responsible for the conceptualization, validation, resources, data curation, software development, and project administration. D. H. Le, H. M. Nguyen and P. D. Le jointly contributed to the methodology, formal analysis, investigation, original draft preparation, review and editing, visualization, supervision, and funding acquisition. All authors have read and agreed to the published version of the manuscript.

Conflict of Interest

The authors declared no potential conflicts of interest with respect to the research, authorship, and/or publication of this article.

References

[1] S. Kenu, R. Uhunmwangho, and K. Okedu, "Harnessing solar and wind power for hybrid stand-alone energy system: The case of coastline communities in Delta State of Southern Nigeria," International Journal of Smart Grid-ijSmartGrid, vol. 7, no. 1, pp. 25–37, 2023.

[2] M. Yousefzadeh, H. R. Najafi, and H. Eliasi, "State-space modeling and small-signal stability analysis of an independent microgrid with multiple distributed generation resources," International Journal of Smart Grid-ijSmartGrid, vol. 8, no. 1, pp. 1–11, 2024.

LVDC microgrid against various faults. In summary, the proposed statistical and adaptable fault protection method can successfully characterize if an event is either a case of abnormal dynamic operation or an actual fault (e.g. a direct/low-impedance P2P fault or a high-impedance P2G fault), in other words, more accuracy in the detection of different faults in the off-grid small-scaled LVDC microgrid. In the future, the authors will design a prototype of DC-microgrid relays (DCMGR) to implement the developed novel protection algorithm. The DCMGR will be a unified protection

[3] S. Sahoo and S. Mishra, "A distributed finite-time secondary average voltage regulation and current sharing controller for DC microgrids," IEEE Transactions on Smart Grid, vol. 10, no. 1, pp. 282–292, 2017.

[4] V. Kumar, S. R. Mohanty, and S. Kumar, "Event trigger super twisting sliding mode control for DC micro grid with matched/unmatched disturbance observer," IEEE Transactions on Smart Grid, vol. 11, no. 5, pp. 3837–3849, 2020.

[5] R. M. Cuzner and G. Venkataramanan, "The status of DC micro-grid protection," 2008 IEEE Industry Applications Society Annual Meeting, pp. 1–8, 2008.

[6] M. Saeedifard, M. Graovac, R. F. Dias, and R. Iravani, "DC power systems: Challenges and opportunities," IEEE PES General Meeting, pp. 1–7, 2010.

[7] S. Augustine, J. E. Quiroz, M. J. Reno, and S. Brahma, "DC microgrid protection: Review and challenges," 2018.

[8] M. E. Baran and N. R. Mahajan, "Overcurrent protection on voltage-source-converter-based multiterminal DC distribution systems," IEEE Transactions on Power Delivery, vol. 22, no. 1, pp. 406–412, 2006.

[9] D. M. Bui, S.-L. Chen, C.-H. Wu, K.-Y. Lien, C.-H. Huang, and K.-K. Jen, "Review on protection coordination strategies and development of an effective protection coordination system for DC microgrid," 2014 IEEE PES Asia-Pacific Power and Energy Engineering Conference (APPEEC), pp. 1–10, 2014.

[10] K. A. Saleh, A. Hooshyar, and E. F. El-Saadany, "Hybrid passive-overcurrent relay for detection of faults in low-voltage DC grids," IEEE Transactions on Smart Grid, vol. 8, no. 3, pp. 1129–1138, 2015.

[11] G. S. Ov and S. Hemamalini, "Review on microgrid and its protection strategies," International Journal of Renewable Energy Research, vol. 6, no. 4, pp. 1574–1587, 2016.

[12] A. Meghwani, S. Srivastava, and S. Chakrabarti, "A non-unit protection scheme for DC microgrid based on local measurements," IEEE Transactions on Power Delivery, vol. 32, no. 1, pp. 172–181, 2016.

[13] H. R. Baghaee, M. Mirsalim, G. B. Gharehpetian, and H. A. Talebi, "A new current limiting strategy and fault

model to improve fault ride-through capability of inverter interfaced DERs in autonomous microgrids," Sustainable Energy Technologies and Assessments, vol. 24, pp. 71–81, 2017.

[14] H. R. Baghaee, M. Mirsalim, G. B. Gharehpetian, and H. A. Talebi, "MOPSO/FDMT-based Pareto-optimal solution for coordination of overcurrent relays in interconnected networks and multi-DER microgrids," IET Generation, Transmission & Distribution, vol. 12, no. 12, pp. 2871–2886, 2018.

[15] A. Shabani and K. Mazlumi, "Evaluation of a communication-assisted overcurrent protection scheme for photovoltaic-based DC microgrid," IEEE Transactions on Smart Grid, vol. 11, no. 1, pp. 429–439, 2019.

[16] C. Srivastava and M. Tripathy, "Novel adaptive fault detection strategy in DC microgrid utilizing statistical-based method," IEEE Transactions on Industrial Informatics, vol. 19, no. 5, 2022.

[17] A. Meghwani, S. C. Srivastava, and S. Chakrabarti, "A non-unit protection scheme for DC microgrid based on local measurements," IEEE Transactions on Power Delivery, vol. 32, no. 1, pp. 172–181, 2016.

[18] L. Tang and B.-T. Ooi, "Locating and isolating DC faults in multi-terminal DC systems," IEEE Transactions on Power Delivery, vol. 22, no. 3, pp. 1877–1884, 2007.

[19] J.-D. Park, J. Candelaria, L. Ma, and K. Dunn, "DC ring-bus microgrid fault protection and identification of fault location," IEEE Transactions on Power Delivery, vol. 28, no. 4, pp. 2574–2584, 2013.

[20] M. Reis, "Optimization of DC feeder rate of rise overcurrent protection settings using delta i cumulative distribution," 2004 IEEE Industrial and Commercial Power Systems Technical Conference, pp. 63–66, 2004.

[21] D.-M. Bui, C.-H. Wu, S.-L. Chen, C.-H. Huang, and K.-Y. Lien, "Installation on a community-sized DC microgrid system and suggestion on a DC short-circuit test procedure," 2014, pp. 1819–1825.

[22] P. D. Le, D. M. Bui, and T. D. Nguyen, "Dynamic and transient responses of a low-voltage DC microgrid with considering multiple battery-supercapacitor-based energy storage configurations," International Journal of Sustainable Energy, vol. 9, no. 1, 2021.

[23] D. M. Bui, P. D. Le, and T. D. Nguyen, "Staged fault tests to validate a fast protection system of low-voltage DC microgrids," 2021 International Conference on Electrical, Computer, Communications and Mechatronics Engineering (ICECCME), pp. 1–6, 2021.

[24] I. E. A. Davidson and E. Buraimoh, "Modelling of a photovoltaic-based grid supporting microgrid and fault ride-through control application," International Journal of Smart Grid-ijSmartGrid, vol. 7, no. 2, pp. 69–83, 2023.

[25] M. U. Raza, I. Raza, Z. Maqbool, B. Masih, and F. Iqbal, "An overview of the topologies of DC circuit breakers in DC microgrids," International Journal of Smart Grid-ijSmartGrid, vol. 7, no. 4, pp. 178–188, 2023.

[26] O. V. G. Swathika, "LUT assisted adaptive overcurrent protection of reconfigurable microgrids," International Journal of Smart Grid-ijSmartGrid, vol. 2, no. 1, pp. 13–26, 2018.

[27] Y. N. L. de Marco, T. Zheng, and S. Nikolovski, "Overcurrent protection assessment with high PV penetration in a distribution network," International Journal of Renewable Energy Research, vol. 8, no. 1, pp. 396–406, 2018.

[28] A. Meghwani, S. Chakrabarti, S. C. Srivastava, and S. Anand, "Analysis of fault characteristics in DC microgrids for various converter topologies," 2017 IEEE Innovative Smart Grid Technologies - Asia (ISGT-Asia), pp. 1–6, 2017.

[29] T. C. Kuo, T. T. Pham, P. T. Huang, H. T. Nguyen, D. M. Bui, and P. D. Le, "Reliability analysis of PV generating systems in the islanded DC microgrid under dynamic and transient operation," IET Renewable Power Generation, vol. 16, no. 5, pp. 988–1026, 2022.

[30] G. K. Rao and P. Jena, "Unit protection of tapped line DC microgrid," IEEE Journal of Emerging and Selected Topics in Power Electronics, vol. 10, no. 4, pp. 4680–4689, 2022.

[31] L. Kong and H. Nian, "Fault detection and location method for mesh-type DC microgrid using Pearson correlation coefficient," IEEE Transactions on Power Delivery, vol. 36, no. 3, pp. 1428–1439, 2020.

[32] G. K. Rao and P. Jena, "Fault detection in DC microgrid based on the resistance estimation," IEEE Systems Journal, vol. 16, no. 1, pp. 1009–1020, 2021.

[33] G. K. Rao and P. Jena, "A novel fault identification and localization scheme for bipolar DC microgrid," IEEE Transactions on Industrial Informatics, vol. 19, no. 12, 2023.

[34] S. Ravyts, G. Van den Broeck, L. Hallemans, M. Dalla Vecchia, and J. Driesen, "Fuse-based short-circuit protection of converter controlled low-voltage DC grids," IEEE Transactions on Power Electronics, vol. 35, no. 11, pp. 11694–11706, 2020.

[35] S. A. Saleh, S. Kanukollu, and A. Al-Durra, "Phaselet transform-based digital ground fault protection of grid-connected photovoltaic systems," IEEE Transactions on Industry Applications, vol. 59, no. 5, 2023.

[36] J.-S. Kim, E.-C. Lee, and S.-Y. Yun, "Protection system for LVDC distribution networks using a fault current-limiting converter and protection zones," IEEE Access, vol. 11, 2023.